

Inflating 2D Convolution Weights for Efficient Generation of 3D Medical Images

Yanbin Liu, Girish Dwivedi, Farid Boussaid, Frank Sanfilippo, Makoto Yamada, *Member, IEEE*,
and Mohammed Bennamoun, *Senior Member, IEEE*

Abstract—The generation of three-dimensional (3D) medical images can have great application potential since it takes into account the 3D anatomical structure. There are two problems, however, that prevent effective training of a 3D medical generative model: (1) 3D medical images are very expensive to acquire and annotate, resulting in an insufficient number of training images, (2) a large number of parameters are involved in 3D convolution. To address both problems, we propose a novel GAN model called *3D Split&Shuffle-GAN*. In order to address the 3D data scarcity issue, we first pre-train a two-dimensional (2D) GAN model using abundant image slices and inflate the 2D convolution weights to improve initialization of the 3D GAN. Novel 3D network architectures are proposed for both the generator and discriminator of the GAN model to significantly reduce the number of parameters while maintaining the quality of image generation. A number of weight inflation strategies and parameter-efficient 3D architectures are investigated. Experiments on both heart (Stanford AIMI Coronary Calcium) and brain (Alzheimer's Disease Neuroimaging Initiative) datasets demonstrate that the proposed approach leads to improved 3D images generation quality with significantly fewer parameters.

Index Terms—Generative adversarial networks, weight inflation, efficient neural networks, three-dimensional medical images

I. INTRODUCTION

WITH the availability of large-scale annotated datasets like ImageNet [1], convolution neural networks (CNNs) have achieved unprecedented success in computer vision [2]. Benefiting from CNNs, medical imaging research has made great advancements in the classification [3], segmentation [4], detection [5], and registration [6] of two-dimensional

(2D) medical images. However, 3D medical image research is lagging behind due to the lack of large-scale 3D medical image datasets. As a result of the complex collection procedure, expert annotation, and privacy concerns and patient consent, it is challenging to build a large-scale, 3D medical dataset similar to ImageNet.

One widely-used solution for the data-deficit of medical images is Generative Adversarial Networks (GANs) [7]. These networks create high-quality synthetic images to mimic realistic data distributions. An example is the use of GANs with Wasserstein distance as well as perceptual loss for low-dose CT image denoising [8]. A cyclic loss GAN was used by [9] to reconstruct MRI images. Using cycle-consistent GANs, [10] translated MR images to CT images. Albeit effective in mitigating the data-deficit challenge, most existing GANs based methods are designed for 2D medical image generation. Therefore, they do not incorporate information about the 3D anatomical structure. Various medical applications require the 3D anatomical structure, including calcium scoring [11] of cardiac CT Coronary Angiograms (CTCAs), and brain tumor segmentation [12]. Unfortunately, there are two practical issues that hinder the effective training of the 3D medical generative model, preventing the use of GANs in 3D medical imaging.

First of all, there are usually insufficient 3D medical images to train effective 3D generative models from scratch. The effective training of 3D CNNs with natural videos, relies on large-scale datasets, such as Moments in Time [13] with 1 million short videos, and Kinetics [14] with 750k video clips. In comparison, medical datasets contain far fewer 3D images. For example, Stanford AIMI Coronary Calcium (COCA) dataset [15] only contains 787 CTCAs. To generate 3D images, [16] used 991 brain MRI images from the Alzheimer's Disease Neuroimaging Initiative (ADNI) dataset [17]. Training an effective 3D generative model from scratch is difficult with such small datasets of 3D medical images.

Secondly, 3D convolution layers have a large number of parameters, making training time slow and prone to overfitting. As a result of 3D convolution, weight parameters take on an additional dimension. For example, the conventional 3×3 convolution expands to $3 \times 3 \times 3$ in the 3D case. Adding the third dimension allows the modeling of the 3D anatomical structure, but it also involves the introduction of an excessive number of parameters and computations, resulting in the slower training. Moreover, the model is prone to overfitting due to the contrast between the large number of parameters

(Corresponding author: Mohammed Bennamoun)

Yanbin Liu is with the UWA centre for medical research, The University of Western Australia, Perth, WA, 6009 Australia.

Girish Dwivedi is jointly with School of Medicine, The University of Western Australia, Harry Perkins Institute of Medical Research, and Department of Cardiology, Fiona Stanley Hospital, Perth, WA 6009, Australia.

Farid Boussaid is with the Department of Electrical, Electronic and Computer Engineering, The University of Western Australia, Perth, WA 6009, Australia.

Frank Sanfilippo is with School of Population and Global Health, The University of Western Australia, Perth, WA 6009, Australia.

Makoto Yamada is with Okinawa Institute of Science and Technology, Okinawa 904-0495, Japan.

Mohammed Bennamoun is with the Department of Computer Science and Software Engineering, The University of Western Australia, Perth, WA 6009, Australia. (e-mail: mohaammed.bennamoun@uwa.edu.au)

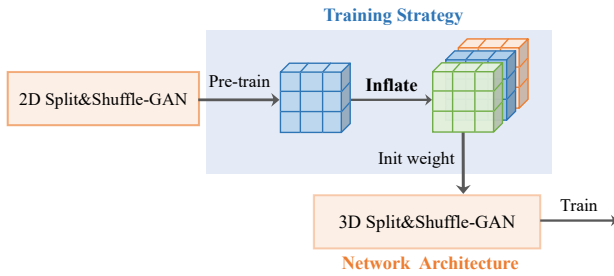


Fig. 1: The general pipeline of our 3D generation model, which includes our contribution to both the training strategy (inflate 2D weights, colored in blue) as well as the network architecture (Split&Shuffle GAN, colored in orange).

and the small number of 3D training images.

To address the above two problems, we propose a novel GAN model, dubbed **3D Split&Shuffle-GAN** for effective and efficient 3D medical image generation. The proposed model improves existing state-of-the-art GANs (e.g., StyleGAN2 [18]) from two perspectives: training strategy and network architecture (see Figure 1).

The proposed training strategy takes advantage of the availability of 2D image slices to train a 2D GAN model. It then inflates the 2D weights to initialize the 3D GAN model. As the 3D GAN model is initialized with informative 2D weights, it is able to focus more on 3D anatomy, which results in a better generation of 3D image. By design, the 2D GAN shares the similar architecture as the 3D GAN, with the exception of the additional convolution dimension (e.g., 3×3 convolution vs. $3 \times 3 \times 3$ convolution). This enables the 2D weights to be seamlessly expanded to 3D using the weight inflation technique [19]. Since the original inflation was designed for classification models rather than generative models, we evaluate five new inflation variants through extensive experiments to determine the most suitable one for the task of 3D image generation.

For the network architecture, we devise novel Channel Split&Shuffle modules to improve both the generator and discriminator networks. For the generator, since the state-of-the-art style-based models (e.g., StyleGAN2) incorporate style vectors into convolution weights as a modulated convolution, efficient convolution operations (e.g., depthwise separable convolution [20] or group convolution [21]) cannot be directly adopted. This is mitigated by our Split&Shuffle module, which splits the feature channels into two equal branches and performs a modulated 3D convolution for each branch. Then, the output channels are concatenated and shuffled to encourage feature exchanges. With this design, the number of parameters of the generator is reduced by a factor of 2. For the discriminator, the number of parameters is further reduced by nearly a factor of 4, by replacing one of the $3 \times 3 \times 3$ convolutions with $1 \times 1 \times 1$ convolution. Although the number of parameters for both the generator and discriminator is significantly reduced, the devised modules achieve a much better performance than the original one. Under the extremely data-deficit challenges of generating 3D medical images, our parameter-efficient model is less likely to overfit than the

original model.

To demonstrate the effectiveness of the training strategy and network architecture, we investigated five novel weight inflation variants as well as five network design choices on the heart dataset, i.e., Stanford AIMI Coronary Calcium (COCA). In addition, we performed experiments on the brain dataset (i.e., Alzheimer’s Disease Neuroimaging Initiative (ADNI)) to demonstrate the general applicability of our method.

To summarize, this paper makes the following contributions to the 3D medical image generation:

- A novel 3D Split&Shuffle-GAN model for 3D medical image generation is proposed, and new inflation strategies are developed to facilitate training of 3D medical generation models.
- Parameter-efficient Channel Split&Shuffle modules are developed for both the generator and discriminator networks, which reduces the number of parameters (by a factor of 2+) and improves generation quality (FID).
- We conducted comprehensive experiments to verify the effectiveness of the inflation strategy and network architecture. We achieved the state-of-the-art performance on both the heart and brain datasets.

II. RELATED WORK

A. Generative Models for Medical Imaging

The most popular model for generating synthetic images is the generative adversarial networks (GANs) [7]. The GANs model synthesizes realistic images from a random noise variable and uses a discriminator to distinguish between the synthesized images and the realistic images. The distribution of the synthesized images gradually approaches the distribution of real images with the alternating training of the generator and discriminator. State-of-the-art GANs use the style-based generation technique [18], [21], in which style vectors are generated (for controlling the style of image generation) from a mapping network.

Providing annotations to large numbers of images in the field of medical imaging is a challenging task. The use of GANs is thus naturally adopted to solve a number of medical problems, such as classification, segmentation, registration, and low dose CT denoising. GANs are used by [3] to generate synthetic computed tomography (CT) images for data augmentation to enhance the liver lesion classification performance. RefineGAN [9] proposes a cyclic consistency loss for the modified variant of the deeper generator and discriminator networks so as to deal with the Compressed Sensing MRI (CS-MRI) reconstruction problem. In order to improve the conventional GANs for the low dose CT (LDCT) denoising task, [8] employs two practical methods, namely Wasserstein distance and perceptual loss. A-CycleGAN [10] makes use of variational autoencoding (VAE), attention, and cycle-consistent generative adversarial network (CycleGAN) to improve existing MR-to-CT image translation algorithms.

In spite of the wide range of models and GANs variants proposed for medical imaging problems, most of them only focus on generating 2D images, disregarding the 3D anatomical structure. Only a few attempts have been made to

generate 3D images. Leveraging an α -GAN, [16] utilizes both the variational autoencoder (VAE) and GAN to generate 3D synthetic brain MRI images. The paper [4] proposes a segmentation guided style-based generative adversarial network (SGSGAN) for the synthesis of full-dose PET images, where a style-based generator is directly used for style modulation. By extending StyleGAN2's 2D convolutions to 3D convolutions, [22] proposes 3D-StyleGAN to generate 3D brain MRI images. Since the above methods lift 2D GANs models to 3D in a straightforward manner, the number of parameters increases significantly, making it challenging to train the model effectively. As a result, we propose in this paper both effective training strategies and efficient model architectures to generate 3D medical images using 3D GANs.

B. Training 3D Convolution Neural Networks

A multitude of research efforts have been directed towards 3D CNNs in the field of natural images, especially for the spatio-temporal analysis of videos. The main idea is to introduce a third convolution dimension ($k \times k \times k$) to capture the temporal dependencies for video applications such as action recognition [19]. The training of 3D CNN models usually relies on large-scale video datasets, e.g., Kinetics-700 [14] with 750k video clips, Moments in Time [13] with 1M short videos. However, due to the high annotation costs, patient consent issues, and expert annotation challenges, creating 3D medical image datasets of similar scale is not feasible. As a result, training 3D medical models from scratch is challenging.

Using degenerated 2D spatial information, another line of work contributes to the initialization of 3D convolution weights by utilizing beneficial priors. As an example, [19] proposes an inflation strategy to stack 2D weights for the 3D weights initialization. The video vision Transformer is trained using the central frame initialization strategy in [23]. To our knowledge, no similar initialization technique has been explored in 3D medical GANs. On one hand, the third dimension in video analysis corresponds to temporally varying frames, while the third dimension in medical images describes 3D anatomical structure. On the other hand, the interplay between the discriminator and generator makes training process more complex than that of classification models. In this paper, we consider both the 3D anatomical structure and the interplay between the discriminator and the generator to facilitate the 3D GANs training and architecture design.

C. Parameter-efficient 3D Convolution Neural Networks

3D convolution neural networks are challenged by the large number of parameters included by the additional third dimension. There are two main approaches to addressing this issue: tensor decomposition and efficient module design. In tensor decomposition, the low-rank tensor decomposition algorithms are applied to re-calculate the convolution weights, thereby compressing the network and reducing the number of parameters. For example, Tensor Train is used in [24], CP decomposition is applied in [25], [26], and Tucker decomposition is adopted in [27]. In spite of their mathematical soundness, these methods require specific re-implementation of existing

convolution operations and cannot take advantage of the latest hardware acceleration (e.g., the NVIDIA cudnn library). In efficient module design, various parameter-efficient modules (e.g., bottleneck [28], group convolution, depthwise separable convolution, and pointwise convolution) are devised to replace the original module. These efficient modules are re-arranged and combined to form different network architectures. In MobileNet [20], for example, depthwise separable convolutions are used to construct a lightweight deep architecture for mobile devices. SqueezeNet [29] combines pointwise convolution and regular convolution to form a Fire block. The computation cost of ShuffleNet [30] is reduced by using pointwise group convolution. A comprehensive analysis of these modules can be found in [31].

All above parameter-efficient designs are based on classification models, which cannot be directly and easily adopted in 3D generative models, such as StyleGAN2. StyleGAN2's style modulation mechanism will be destroyed if these modules are trivially adopted. In order to address this issue, we propose customized 3D modules for the style-based generative models to enable parameter-efficient generation of 3D medical images.

III. METHOD

A. StyleGAN2 for 3D Medical Images Generation

1) Overview of StyleGAN2 model:

a) *Mapping Network*: A key difference between style-based generation model (e.g., StyleGAN2) and previous GANs is the introduction of the mapping network f . Specifically, given a latent code $z \in \mathcal{Z}$, $f: \mathcal{Z} \rightarrow \mathcal{W}$ first produces a vector $v \in \mathcal{V}$. The learned affine transform is then applied on v to obtain the per-layer style vectors s for the generator.

b) *Generator*: In the generator, original StyleGAN [21] directly utilizes the style vectors for adaptive instance normalization (AdaIN) on the feature maps, which will cause the characteristic artifacts such as droplet. To mitigate these unrealistic artifacts, StyleGAN2 incorporates the style vectors into the weight modulation (Mod) operation, then apply the demodulation (Demod) to serve as the instance normalization.

$$\text{Modulation: } w'_{ijk} = s_i \cdot w_{ijk}, \quad (1)$$

$$\text{Demodulation: } w''_{ijk} = w'_{ijk} / \sqrt{\sum_{i,k} w'_{i,j,k}{}^2 + \epsilon}, \quad (2)$$

where w, w', w'' are the original, modulated and demodulated convolution weights, s_i is the style vector corresponding to the i -th feature map, j, k iterate the output feature maps and the spatial resolution, ϵ is a small constant to avoid numerical issues. In the above modulation and demodulation operations, the style vectors are directly entangled with convolution weights, which removes the characteristic artifacts while retaining the style controllability. However, this also impedes the straightforward modification to the convolution layers, e.g., depthwise separable convolution (details in Sec. III-C).

c) *Discriminator*: The discriminator of StyleGAN2 introduces a minibatch standard deviation layer to calculate the deviation of a minibatch and concatenate it to the original feature maps. This reduces the dependency within a minibatch to encourage diverse generation.

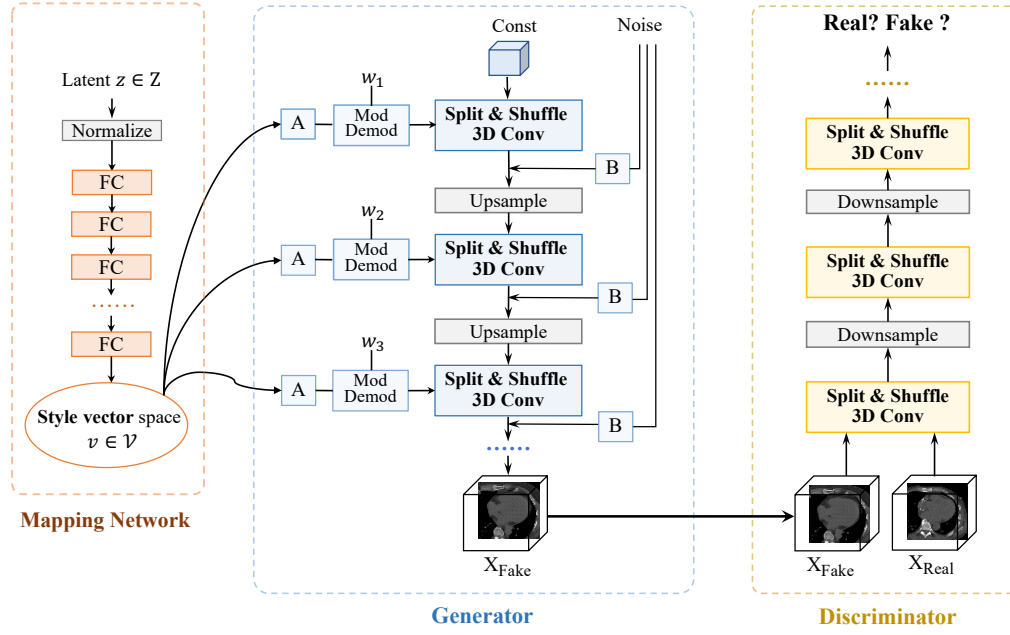


Fig. 2: The overall architecture of the proposed 3D Split&Shuffle-GAN. It is composed of a Mapping Network, a Generator, and a Discriminator. Mapping Network maps a latent variable z to the style vector space \mathcal{V} , and produces the per-layer style vectors with a learned affine transform (A). Generator starts from a constant 3D input. Then it controls the 3D generation styles with the per-layer style vectors and adds in details from the per-channel scaled (B) noise input. Weight Mod&Demod incorporates the style vector into the convolution operation. Discriminator tries to differentiate the real 3D images from the generated fake 3D images. Inside both the Generator and Discriminator, we devise novel **Channel Split&Shuffle** modules for parameter-efficient 3D convolution operation, which are customized for the style-based generation framework.

2) 3D Medical Image Generation: The StyleGAN2 is originally designed for the 2D natural images generation. To apply it for the 3D medical images generation, a straightforward approach [22] is by lifting all the 2D convolution operations to the 3D convolution operations, e.g., expanding the 3×3 convolutions to the $3 \times 3 \times 3$ convolutions. Albeit simple, this approach will significantly increase the number of parameters, thereby posing two practical issues: (1) it will require a large number of 3D images for training, otherwise the model suffering overfitting issue, (2) the largely increased parameter number will slow down both training and generation. However, no existing methods have simultaneously addressed both issues. Therefore, it is non-trivial to improve StyleGAN2 for 3D medical images generation.

In this paper, we deal with the issues from the **training strategy** (Weight Inflation in Sec III-B) and **network architecture** (Split&Shuffle in Sec III-C) perspectives and propose an efficient 3D generative model as shown in Figure 2.

B. Inflating 2D Convolution Weights

This section discusses how to design a training strategy to generate synthetic 3D medical images and overcome the issue of data scarcity. Transfer learning [32] is a widely-used technique to overcome the data paucity of the target task by employing additional external datasets. As an example, ImageNet [1] is used as an external dataset for a variety of tasks, including object detection, and segmentation. In MinGAN [33], knowledge is transferred from GANs to

domains with few images. It is currently difficult to apply the transfer learning technique for 3D GANs models in medical research due to the lack of large datasets and effective transfer learning strategies. 3DSeg-8 dataset [34] has been aggregated from eight datasets to facilitate transfer learning between 3D medical images for liver segmentation and nodule classification. However, there are only tens to hundreds of 3D images of organs/tissues in each dataset in 3DSeg-8, which makes GANs incapable of transferring detailed knowledge. Moreover, the interplay between the generator and discriminator poses a different transfer learning challenge compared to classification tasks with a single network.

Although direct transferring from external datasets is infeasible for 3D medical images generation, we note an interesting and helpful observation: **2D slices in a medical dataset are several magnitudes larger than 3D images**. As an example, Stanford AIMI Coronary Calcium (COCA) [15] contains only 787 CTCA images, but these CTCA images contain 39,281 2D slices. As such, the number of these 2D slices is sufficient to train a 2D generative model such as StyleGAN2. Since 2D and 3D generative models have distinct weights, it is not possible to transfer weights directly from 2D to 3D generative models. As a result, we are naturally drawn to another technique called weight inflation [19], which enables effective 3D network training from the pre-trained 2D weights.

Weight inflation was firstly introduced in [19] for the design and training of 3D video action recognition networks. The method has been applied to both CNNs and Trans-

formers based 3D models [19], [23]. In technical terms, it extends/inflates/copies the 2D convolution weights along the third dimension (e.g., temporal dimension in video) to provide a more favourable initialization for the 3D convolution networks. In order to ensure feasible inflation from 2D weights to 3D models, the 2D and 3D networks must have the same basic structure except for the additional third dimension (e.g., the 3×3 and $3 \times 3 \times 3$ convolutions should have the same number of channels). **To our knowledge, this technique has not been applied to medical image analysis, and in particular to 3D medical image generation.**

Taking into account the application differences between video action recognition and 3D medical image generation, we propose five customized inflation strategies to facilitate the training of 3D StyleGAN2. Here, we set the size of convolution weights to be $3 \times 3 \times 3$, but our strategies can be easily adapted to other weight sizes. Let $w_2 \in \mathbb{R}^{C_I \times C_O \times 3 \times 3}$ denote the pre-trained 2D convolution weights, and $w_3 \in \mathbb{R}^{C_I \times C_O \times 3 \times 3 \times 3}$ denote the corresponding 3D convolution weights. At first, we initialize w_3 from a random Gaussian $\mathcal{N}(0, 0.1)$. Then, the weight w_3 is modified by the following inflation strategies:

- **Inflate-1:** only inflating 1 center dimension.

$$w_3[:, :, 1, :, :] = w_2. \quad (3)$$

- **Inflate-2:** inflating 2 dimensions.

$$w_3[:, :, 0, :, :] = w_2, \quad w_3[:, :, 1, :, :] = w_2. \quad (4)$$

- **Inflate-3:** inflating all 3 dimensions.

$$\begin{aligned} w_3[:, :, 0, :, :] &= w_2, & w_3[:, :, 1, :, :] &= w_2, \\ w_3[:, :, 2, :, :] &= w_2. \end{aligned} \quad (5)$$

- **Inflate-ASC:** inflating the axial, sagittal, and coronal planes of 3D medical views.

$$\begin{aligned} w_3[:, :, 1, :, :] &= w_2, & w_3[:, :, :, 1, :] &= w_2, \\ w_3[:, :, :, :, 1] &= w_2. \end{aligned} \quad (6)$$

- **Inflate-NWI:** the negative weight initialization (NWI) is used here, with the center dimension owing a larger value and the other dimensions owing negative values ($T = 3$).

$$w_3[:, :, i, :, :] = \alpha_i * w_2, \quad \alpha_i = \begin{cases} \frac{2T-1}{T}, & \text{if } i = 1 \\ -\frac{1}{T}, & \text{otherwise} \end{cases} \quad (7)$$

By design, different inflation strategies offer diverse ways of reusing the 2D weights: the reusing degree increases from Inflate-1 to Inflate-3; Inflate-ASC considers the anatomical views; Inflate-NWI modifies Inflate-1 with more attention on the center dimension and negative weights on others. Intuitively, these inflation strategies introduce helpful 2D structure priors through weight initialization, which significantly reduces the training burden of the 3D convolution weights. In this way, by focusing more on the third dimension (for the anatomy learning), the generative model is able to generate high-quality 3D images quickly and efficiently.

C. Efficient 3D Architecture Design

Although inflation strategy mitigates the lack of 3D data in training the 3D GAN model, it still suffers from the large number of model parameters. In this section, we address this issue from the perspective of efficient 3D architecture design.

We observe that most of the parameters in the 3D neural network architecture originate from the 3D convolution operation, which extends the 2D convolution weights to 3D, to model the 3D contextual and anatomical structures (e.g., lifting 3×3 weights to $3 \times 3 \times 3$). Existing efficient 3D architecture designs mainly focus on parameter-efficient 3D convolution. On one hand, factorized high-order CNNs are proposed with different tensor decomposition algorithms such as Tensor-Train (TT) [24], CP decomposition [25], [26], Tucker Decomposition [27]. These methods compress networks and reduce their parameters by applying low-rank tensor decompositions to the high-order weights. On the other hand, driven by the requirements of mobile devices, various parameter-efficient convolution variants are devised and combined into efficient architectures, such as group convolution [2], bottleneck [35], depthwise separable convolution [20]. Group convolution divides the channels into groups and performs convolution only within each group. Bottleneck was introduced in ResNet [35] to reduce the number of channels of the 3×3 convolution by wrapping it with two 1×1 convolutions. With depthwise separable convolutions, the standard convolutions are factorized into a depth-wise convolution (i.e., a group convolution with group number equal to channel number) followed by a 1×1 pointwise convolution.

The above designs were developed to improve the efficiency of various applications, e.g., HO-CPConv [26] for spatio-temporal facial emotion analysis, MobileNet [20] for image classification and object detection, and 3D-MobileNet [31] for video action recognition. **Despite this, the efficient 3D GANs architecture is rarely studied, especially for the state-of-the-art StyleGAN2 model.** We attribute this to two possible reasons: (1) The StyleGAN2 architecture is more delicate than classification models, hindering the straightforward adoption of existing modules such as tensor decomposition, group convolution, or depthwise separable convolution. Specifically, the style vectors are absorbed in the modulation and demodulation operations (Eqs. 1, 2), which sets up hurdles for existing modules. (2) As a result of the interplay between discriminator and generator, GANs training is difficult. It is non-trivial to directly use the same modules for the discriminator and generator in order to achieve best performance.

Based on the above analysis, we propose a unique design that is customized to the StyleGAN2 model for parameter-efficient generation (Figure 3). For the generator, since the direct adoption of existing efficient modules (e.g., group convolution, depthwise separable convolution) will break the entangled structure of the convolution weights and style vectors (Eqs. 1, 2), we equally **Split** the feature maps, using the channel split operation, to undergo two branches. The modulation and demodulation operations w.r.t. the style vectors and convolution weights are individually applied to each branch. Afterwards, the outputs of the two branches are concatenated,

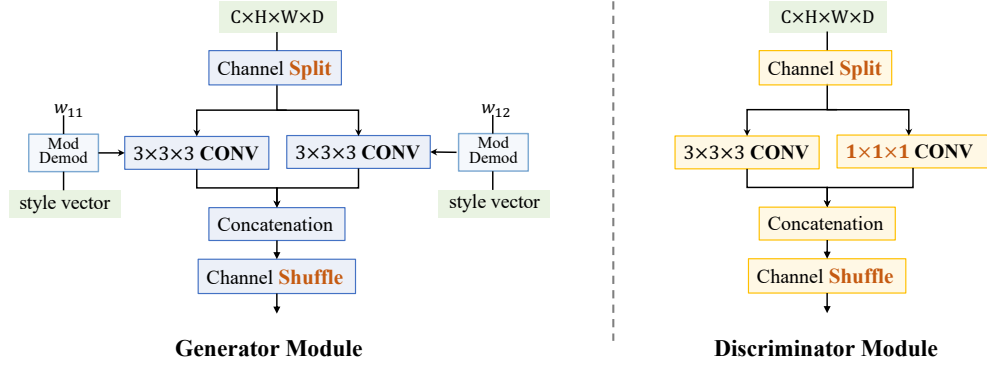


Fig. 3: The proposed Channel Split&Shuffle Convolution Modules for the Generator and Discriminator. The Discriminator module has two differences from the Generator module: the style Mod&Demod and $1 \times 1 \times 1$ Convolution. Overall, the proposed module reduces the number of parameters by a factor of 2 in Generator and nearly by a factor of 4 in Discriminator.

and the **Channel Shuffle** operation is performed, allowing information to be shared between two channels. If the Channel Shuffle operation is not performed, the generator is considered to be two independent networks. Channel Shuffle enables hybrid and diverse pattern combinations across branches to facilitate the image generation quality. For the discriminator, as neither modulation nor demodulation is applied, there is more flexibility in improving the design. Therefore, we devise two asymmetric branches with $3 \times 3 \times 3$ and $1 \times 1 \times 1$ convolutions. The $1 \times 1 \times 1$ convolution leads to a further parameter reduction while compromising the local spatial structure. But this is rectified by the Channel Shuffle operation which exchanges information by shuffling the feature maps of $1 \times 1 \times 1$ and $3 \times 3 \times 3$ convolutions. Overall, the generator enjoys a parameter reduction by a factor of 2 while the discriminator enjoys a parameter reduction by nearly a factor of 4.

We also propose several other parameter-efficient convolution architectures as baselines to verify the Split&Shuffle design's effectiveness. As a result of the modulation and demodulation constraint in the generator, several baselines only modify the discriminator (i.e., D only). All the model variants are listed below:

- **Group Convolution (D only)**, which replaces the convolution in the discriminator with a group convolution.
- **Depthwise Separable Convolution (D only)**, which replaces the convolution in the discriminator with a depthwise separable convolution.
- **Split&Shuffle Convolution (D only)**, which applies the Split&Shuffle module only on the discriminator.
- **Split Convolution**, which applies the channel split without channel shuffle.
- **Split&Shuffle Convolution**, which is our final design.

IV. EXPERIMENTS

A. Datasets and Evaluation Metrics

1) **Datasets:** Stanford AIMI Coronary Calcium (COCA) [15] dataset is used for heart CTCA images. COCA contains 787 3D coronary CT images. Each 3D image has a different number (ranging from 27 to 156) of 2D slices on the axial plane, and they add up to 39,281 axial slices in

total. For brain MRI images, we use the Alzheimer's Disease Neuroimaging Initiative (ADNI) [17] dataset. Specifically, we use 991 T1 structural images from the Cognitively Normal (CN) research group. MR images with non-brain areas are removed by the dataset provider using software FreeSurfer's¹ recon-all function. The processed MR images have 256 slices from all three planes.

2) **Evaluation Metric:** In order to assess the quality of generated images, GANs usually use the Fréchet inception distance (FID) [36] metric, which compares the feature distributions of real and generated images. By default, the Inception V3 network [37] pre-trained with 2D natural images was deployed for feature extraction. However, the method cannot be directly applied to 3D images. As such, taking into account the 3D medical structure, we measure the FID scores on the center slices of axial, sagittal and coronal planes, i.e., *FID-ax*, *FID-sag*, and *FID-cor*. Lastly, we average the three FID scores to obtain *FID-avg* as an overall measurement.

B. Implementation Details

1) **Pre-processing:** Both the COCA and ADNI images are resized to 64×64 using bilinear interpolation in the sagittal and coronal planes. We align the axial slice number of COCA dataset to 32 either by consecutive slice sampling or by zero padding. For ADNI dataset, we directly resize the axial slice number to 64. As a result, the image resolution of COCA and ADNI datasets are $32 \times 64 \times 64$ and $64 \times 64 \times 64$, respectively. The Hounsfield Unit values are clipped to $[-250, 650]$ and then normalized to $[-1, 1]$.

2) **StyleGAN2 architecture:** The base layer (Const in Figure 2) for COCA dataset is set to $2 \times 4 \times 4$, followed by 5 upsampling stages. For ADNI dataset, the base layer is set to $4 \times 4 \times 4$, followed by 5 upsampling stages. The total number of convolution channels is set to 32, with each branch owing 16. Feature dimension of the mapping network is set to 64.

3) **Hyper-parameters:** We follow the StyleGAN2 configuration for training, with the following exceptions: $\gamma = 0.0512$ for R_1 regularization, minibatch = 128, learning rate $\text{lr} = 0.0025$ for training from scratch, $\text{lr} = 0.002$ for inflation initialization.

¹<https://surfer.nmr.mgh.harvard.edu/fswiki>

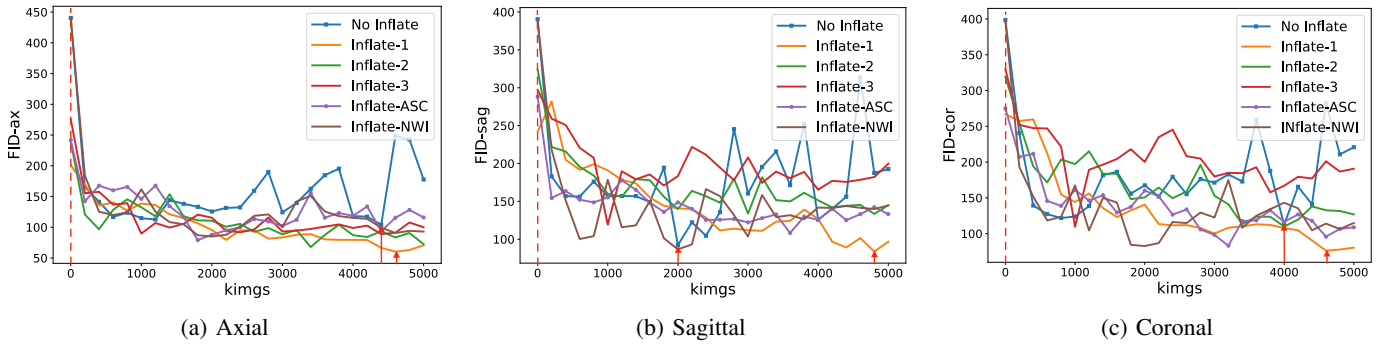


Fig. 4: Performance of different inflation variants during the training process (kimgs). Among all, “Inflate-1” generally obtains good FID scores on all three views. Red arrows show the best FID iterations (kimgs) for “No Inflate” and “Inflate-1”.

For 2D GANs pre-training, the models are fed with 25,000K images in total. While for 3D GANs, they are trained with 5,000K images, since 3D models are slow to train.

C. Inflation and Architecture Analysis

1) Inflation: The first step is to conduct comprehensive experiments to verify that inflation strategies are effective for initializing the 3D generative model. A 2D StyleGAN2 model is pre-trained using all the 39,281 axial slices to obtain the 2-dimensional convolution weights. Since the number of images are sufficient, the 2D model achieves an FID of 7.71. This means that the pre-trained 2D weights capture rich slice-level contextual information to generate high-quality 2D slices. Thus, it verifies the rationale behind inflating 2D pre-trained weights for 3D generative model.

Starting from the same pre-trained 2D weights, we apply all the proposed inflation strategies as well as a “No Inflate” baseline to initialize and train the 3D StyleGAN2 model. The results are shown in Table I. It can be seen that three inflation strategies outperform the “No Inflate” baseline (the other two are comparable), indicating that inflation strategies are generally effective as favourable initialization methods for 3D generative models. “Inflate-1”, which only initializes one center dimension, achieves the best performance (FID-avg) among all inflation variants. Performance gradually degrades as more weights are initialized from 2D weights (“Inflate-2” and “Inflate-3”). We conjecture that the overly inflated 3D weights will prevent the model from freely learning the third dimensional anatomical structure. “Inflate-ASC” and “Inflate-NWI” perform slightly worse than “Inflate-1”.

To understand the training dynamics of various inflation strategies, we plot the FID scores with respect to the training iteration (measured by the number of 1,000 training images, i.e., kimgs) in Figure 4. In general, “Inflate-1” achieves the best performance during training, consistent with Table I. Most inflation variants achieve significantly better FID scores than the baseline at the start of training (i.e., kimgs=0), demonstrating the effectiveness of 2D weights priors in training StyleGAN2. “Inflate-NWI” initially performs worse because it modifies the original 2D weights, but in the end it outperforms the baseline since the prior informative 2D weights have made a big difference.

TABLE I: Performance of different inflation variants.

Model	FID-ax	FID-sag	FID-cor	FID-avg
No Inflate	104	92	112	102.7
Inflate-1	60	83	76	73.0
Inflate-2	68	133	110	103.7
Inflate-3	89	119	110	106.0
Inflate-ASC	79	108	83	90.0
Inflate-NWI	85	87	83	85.0

TABLE II: Inflation on Generator (G) and Discriminator (D).

Model	Module	FID-ax	FID-sag	FID-cor	FID-avg
Inflate-1	G	105	82	88	91.7
	D	85	94	104	94.3
	G&D	60	83	76	73.0
Inflate-ASC	G	93	96	94	94.3
	D	123	113	127	121.0
	G&D	79	108	83	90.0
Inflate-NWI	G	85	91	94	90.0
	D	90	92	98	93.3
	G&D	85	87	83	85.0

In Figure 5, we randomly generate the axial/sagittal/coronal slices of CT images for both the “No Inflate” baseline and our best variant “Inflate-1” to intuitively investigate why inflation strategy works. Specifically, we show the generated images from the initial training iteration (i.e., the dashed lines in Figure 4) and the best training iteration (i.e., the red arrows in Figure 4). It is easy to observe that with inflation as a favorable initialization, the generated images already show meaningful anatomical structures even before training (e.g., FID-ax=201). By contrast, the randomly initialized “No Inflate” generates blurry meaningless images before training (FID-ax=440). This comparison provides an intuitive explanation for the working mechanism of the inflation strategy: with effective inflation, the 3D generative model can inherit meaningful 2D anatomical priors for better subsequent training. Furthermore, starting from better initial weights, the inflated model (“Inflate-1”) is trained to achieve superior generation performance compared to the “No Inflate” baseline (e.g., FID-ax=60 vs FID-ax=104).

StyleGAN2’s discriminator and generator have different structures by design. This motivates us to examine how inflation affects the discriminator and the generator. Specifically, we select the three best inflation variants (“Inflate-1”, “Inflate-ASC”, and “Inflate-NWI”) and perform three sets

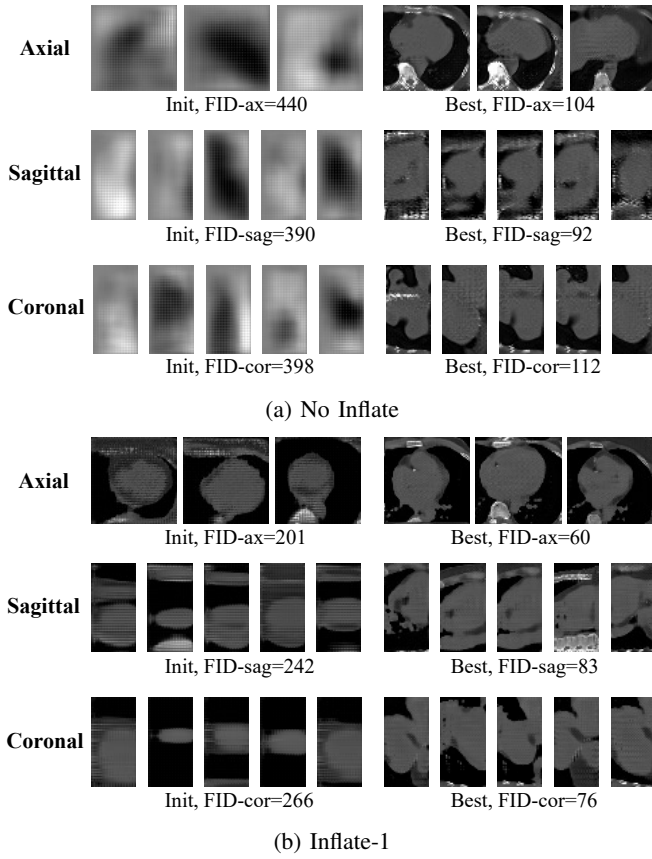


Fig. 5: Generated images from the initial training (dashed lines in Fig. 4) and the best (red arrows in Fig. 4) training iterations. (a) With random weights as an initialization (No Inflate), the initial generated images are meaningless. (b) With inflated weights as a favorable initialization (Inflate-1), the initial generated images already show basic anatomy structures.

of experiments: inflating the generator only (G), inflating the discriminator only (D), and inflating both the generator and discriminator (G&D, default). This analysis reveals two observations: (1) inflating the entire model (G&D) always achieves the best performance, (2) the generator plays a more important role in the inflation strategy, which is reasonable because the generator is responsible for generating images with the style vectors to control the generation.

2) Architecture: Our next step is to conduct experiments to comprehensively investigate efficient 3D architectural designs. At first, all model variants including the baseline are trained from scratch without weight inflation. The FID values and number of parameters are shown in Table III. The models with a “-D” suffix apply efficient modules only on the discriminator, thus only leading to a slightly reduced parameter number (e.g., 0.434M vs 0.600M). “Group-D”, “Depthwise-D”, and “Split&Shuffle-D” have different number of parameters because the architectures are different. By contrast, the proposed “Split&Shuffle” design reduces more than half of the parameters compared to the baseline (0.291M vs 0.600M).

With regards to generation performance, the proposed “Split&Shuffle” architecture achieves the better FID-avg with

TABLE III: Parameter and performance comparison on different architectures. Models with “-D” mean only the discriminator owns the modified architecture.

Model	#param	FID-ax	FID-sag	FID-cor	FID-avg
Baseline	0.600M	104	92	112	102.7
Group-D	0.434M	80	130	105	105.0
Depthwise-D	0.367M	67	136	117	106.7
Split&Shuffle-D	0.416M	84	121	118	107.7
Split	0.291M	109	151	146	135.3
Split&Shuffle	0.291M	85	113	91	96.3

TABLE IV: Model performance when inflation strategy (“Inflate-1”) is applied to different architectures. FID-2D denotes the pre-trained 2D model performance.

Model	#param	FID-2D	FID-ax	FID-sag	FID-cor	FID-avg
Baseline	0.600M	7.7	60	83	76	73.0
Group-D	0.434M	10.9	78	76	76	76.7
Depthwise-D	0.367M	14.0	87	129	84	100.0
Split&Shuffle-D	0.416M	10.6	95	112	101	102.7
Split	0.291M	11.6	120	144	106	123.3
Split&Shuffle	0.291M	12.2	46	66	63	58.3

the least number of parameters, proving its efficiency and effectiveness. All the “-D” models produce similar results to the baseline, indicating that modifying just the discriminator has little influence on the generation quality. Note that owing the same number of parameters, “Split” performs much worse than the “Split&Shuffle” design. As a result, the Channel Shuffle in Figure 3 plays a crucial role in ensuring the performance of the generation.

Then, we examine how efficient architectures can be combined with inflation strategies for further performance enhancement. Specifically, we adopt the best inflation strategy “Inflate-1” and apply it to all the models in Table III. The results are shown in Table IV. In this experiment, each individual model has its own pre-trained 2D weights due to the differences in architecture. Table IV demonstrates that all models achieve good FID-2D values, once again verifying the rationale for inflating informative 2D weights for 3D GANs training. Since the number of 2D image slices is sufficient for 2D pre-training, “Baseline” with the largest number of parameters achieves the best FID-2D. However, for the final 3D training, our “Split&Shuffle” model achieves the best performance (FID-avg) with the least number of parameters. **Compared with the “Baseline” model, “Split&Shuffle” reduces the FID-avg by 24.4 with only 48.5% of the parameters.** As to the discriminator only variants with suffix “-D”, they are much worse than the “Inflate-1” baseline. Without channel shuffle operation, “Split” achieves the worst performance, again showing the indispensable role of channel shuffle in our architecture design.

The visualization of the generated image slices (Split&Shuffle + Inflation) are shown in Figure 6. Similar to Figure 5b, initial images are generated with reasonable heart anatomy, and realistic images are generated based on the best training snapshot.

D. Comparison with the State-of-the-art Methods

Finally, we compare the performance of our method with the published 3D generative models in Table V (COCA)

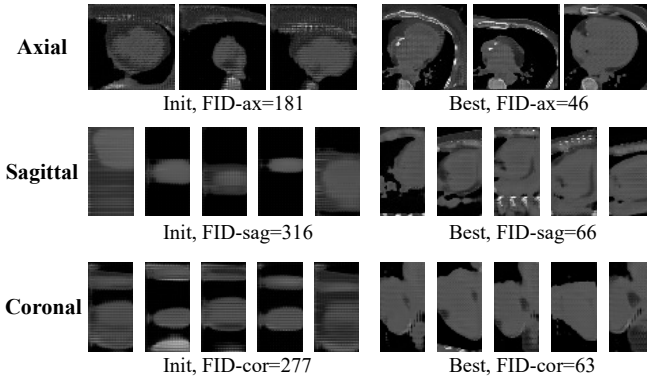


Fig. 6: Generated images from the initial and the best training of our Split&Shuffle model with inflation. By utilizing 2D inflation, we are able to display good heart anatomy initially, and we are able to generate realistic images (FID, Best).

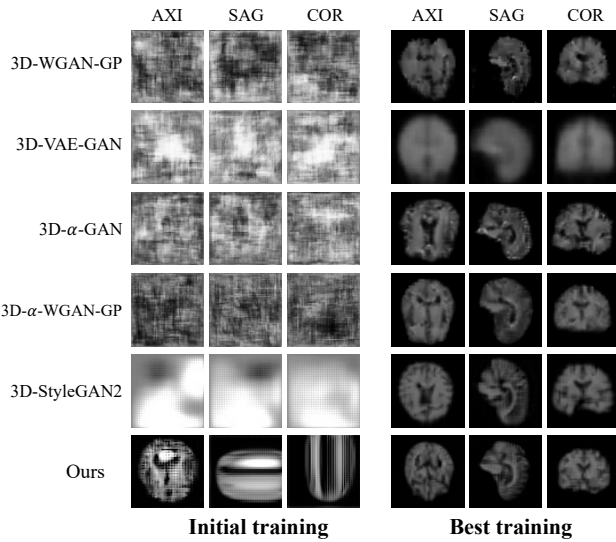


Fig. 7: Generated images from the initial training and the best training on the brain ADNI dataset. Our method shows good initial brain anatomy, especially for the axial view.

and Table VI (ADNI). The comparison methods include the following 3D generation baselines:

- 3D-WGAN-GP [38], a 3D extension of Wasserstein GAN with Gradient Penalty to alleviate training instability.
- 3D-VAE-GAN [39], consisting of an encoder, a decoder and a discriminator.
- 3D- α -GAN [40], applying the code discriminator and encoder on top of the conventional GANs to alleviate the collapse and blurriness.
- 3D- α -WGAN-GP [41], utilizing both the α -GAN structure and the WGAN-GP loss.
- 3D-StyleGAN2 [22], a direct 3D extension of the 2D StyleGAN2 model.

On both the heart and brain datasets, the proposed method outperforms all the state-of-the-art methods with a large margin, demonstrating its effectiveness. Among all comparison methods, the first four baselines have a much greater number of parameters than our method, but achieve inferior per-

TABLE V: Comparison with the state-of-the-art methods on the COCA (heart) dataset.

Model	#param	FID-ax	FID-sag	FID-cor	FID-avg
3D-WGAN-GP	1.399M	191	223	191	201.7
3D-VAE-GAN	6.389M	196	281	272	249.7
3D- α -GAN	2.811M	91	88	80	86.3
3D- α -WGAN-GP	2.811M	70	86	69	75.0
3D-StyleGAN2	0.600M	104	92	112	102.7
Split&Shuffle (Ours)	0.291M	46	66	63	58.3

TABLE VI: Comparison with the state-of-the-art methods on the ADNI (brain) dataset.

Model	#param	FID-ax	FID-sag	FID-cor	FID-avg
3D-WGAN-GP	1.817M	161	161	231	184.3
3D-VAE-GAN	11.001M	167	122	224	171.0
3D- α -GAN	3.635M	73	77	99	83.0
3D- α -WGAN-GP	3.635M	74	72	87	77.7
3D-StyleGAN2	0.633M	114	89	99	100.7
Split&Shuffle (Ours)	0.325M	65	67	82	71.3

mance. Although 3D-StyleGAN2 has approximately twice as many parameters as our method, it still performs much worse. Because the 3D medical generation lacks sufficient 3D training images, most baselines are short of sufficient 3D training images, leading to the inferior performance. As an alternative, our method makes use of both the weight inflation and Split&Shuffle designs in order to mitigate the reliance on a large number of 3D images for training.

Figure 7 shows examples of brain slices generated using all comparison methods. Our method generates high-quality brain slices on three planes. Because of the random weight initialization, the comparison methods generate random images at the start of the training process without any meaningful patterns. Due to its training on sufficient 2D axial slices, our model exhibits good anatomy right at the beginning. Combining our Split&Shuffle design with this anatomy prior allows our model to generate better results with fewer parameters.

V. CONCLUSION AND DISCUSSION

The purpose of this paper is to address the important problem of generating reliable synthetic three-dimensional (3D) medical images. The lack of annotated 3D data and inefficient parameter setting hinder the effective training of the 3D medical generative models. A novel GAN model (i.e., 3D Split&Shuffle-GAN) is proposed to remedy these problems from two perspectives: training strategy and network architecture. For training strategy, we use the weight inflation technique to pre-train a 2D GAN model and inflate the 2D convolution weights as a favorable method for initializing a 3D GAN model. For network architecture, we devise parameter-efficient Channel Split&Shuffle modules for the discriminator and generator of the GAN. We conducted comprehensive experiments to determine the best weight inflation variant and network architecture design. The effectiveness of our method is verified on both the heart and brain datasets. Further exploration of network weight initialization strategies beyond inflation and design of new architectures will be undertaken in the future.

REFERENCES

- [1] O. Russakovsky, J. Deng, H. Su, J. Krause, S. Satheesh, S. Ma, Z. Huang, A. Karpathy, A. Khosla, M. Bernstein *et al.*, "Imagenet large scale visual recognition challenge," *International journal of computer vision*, vol. 115, no. 3, pp. 211–252, 2015.
- [2] A. Krizhevsky, I. Sutskever, and G. E. Hinton, "Imagenet classification with deep convolutional neural networks," *Advances in neural information processing systems*, vol. 25, 2012.
- [3] M. Frid-Adar, E. Klang, M. Amitai, J. Goldberger, and H. Greenspan, "Synthetic data augmentation using gan for improved liver lesion classification," in *2018 IEEE 15th international symposium on biomedical imaging (ISBI 2018)*. IEEE, 2018, pp. 289–293.
- [4] Y. Zhou, Z. Yang, H. Zhang, I. Eric, C. Chang, Y. Fan, and Y. Xu, "3d segmentation guided style-based generative adversarial networks for pet synthesis," *IEEE Transactions on Medical Imaging*, 2022.
- [5] E. H. Nguyen, H. Yang, R. Deng, Y. Lu, Z. Zhu, J. T. Roland, L. Lu, B. A. Landman, A. B. Fogo, and Y. Huo, "Circle representation for medical object detection," *IEEE Transactions on Medical Imaging*, 2021.
- [6] T. Makela, P. Clarysse, O. Sipila, N. Pauna, Q. C. Pham, T. Katila, and I. E. Magnin, "A review of cardiac image registration methods," *IEEE Transactions on medical imaging*, vol. 21, no. 9, pp. 1011–1021, 2002.
- [7] I. Goodfellow, J. Pouget-Abadie, M. Mirza, B. Xu, D. Warde-Farley, S. Ozair, A. Courville, and Y. Bengio, "Generative adversarial nets," *Advances in neural information processing systems*, vol. 27, 2014.
- [8] Q. Yang, P. Yan, Y. Zhang, H. Yu, Y. Shi, X. Mou, M. K. Kalra, Y. Zhang, L. Sun, and G. Wang, "Low-dose ct image denoising using a generative adversarial network with wasserstein distance and perceptual loss," *IEEE transactions on medical imaging*, vol. 37, no. 6, pp. 1348–1357, 2018.
- [9] T. M. Quan, T. Nguyen-Duc, and W.-K. Jeong, "Compressed sensing mri reconstruction using a generative adversarial network with a cyclic loss," *IEEE transactions on medical imaging*, vol. 37, no. 6, pp. 1488–1497, 2018.
- [10] V. Kearney, B. P. Ziemer, A. Perry, T. Wang, J. W. Chan, L. Ma, O. Morin, S. S. Yom, and T. D. Solberg, "Attention-aware discrimination for mr-to-ct image translation using cycle-consistent generative adversarial networks," *Radiology: Artificial Intelligence*, vol. 2, no. 2, p. e190027, 2020.
- [11] P. Greenland, M. J. Blaha, M. J. Budoff, R. Erbel, and K. E. Watson, "Coronary calcium score and cardiovascular risk," *Journal of the American College of Cardiology*, vol. 72, no. 4, pp. 434–447, 2018.
- [12] F. Isensee, P. Kickingereder, W. Wick, M. Bendszus, and K. H. Maier-Hein, "Brain tumor segmentation and radiomics survival prediction: Contribution to the brats 2017 challenge," in *International MICCAI Brainlesion Workshop*. Springer, 2017, pp. 287–297.
- [13] M. Monfort, A. Andonian, B. Zhou, K. Ramakrishnan, S. A. Bargal, T. Yan, L. Brown, Q. Fan, D. Gutfreund, C. Vondrick *et al.*, "Moments in time dataset: one million videos for event understanding," *IEEE transactions on pattern analysis and machine intelligence*, vol. 42, no. 2, pp. 502–508, 2019.
- [14] J. Carreira, E. Noland, C. Hillier, and A. Zisserman, "A short note on the kinetics-700 human action dataset," *arXiv preprint arXiv:1907.06987*, 2019.
- [15] S. AIMI. (2022) Coca - coronary calcium and chest ct's dataset. [Online]. Available: <https://stanfordaimi.azurewebsites.net/datasets/e8ca74dc-8dd4-4340-815a-60b41f6cb2aa>
- [16] G. Kwon, C. Han, and D.-s. Kim, "Generation of 3d brain mri using auto-encoding generative adversarial networks," in *International Conference on Medical Image Computing and Computer-Assisted Intervention*. Springer, 2019, pp. 118–126.
- [17] M. W. Weiner, D. P. Veitch, P. S. Aisen, L. A. Beckett, N. J. Cairns, R. C. Green, D. Harvey, C. R. Jack Jr, W. Jagust, J. C. Morris *et al.*, "The alzheimer's disease neuroimaging initiative 3: Continued innovation for clinical trial improvement," *Alzheimer's & Dementia*, vol. 13, no. 5, pp. 561–571, 2017.
- [18] T. Karras, S. Laine, M. Aittala, J. Hellsten, J. Lehtinen, and T. Aila, "Analyzing and improving the image quality of stylegan," in *Proceedings of the IEEE/CVF conference on computer vision and pattern recognition*, 2020, pp. 8110–8119.
- [19] J. Carreira and A. Zisserman, "Quo vadis, action recognition? a new model and the kinetics dataset," in *proceedings of the IEEE Conference on Computer Vision and Pattern Recognition*, 2017, pp. 6299–6308.
- [20] A. G. Howard, M. Zhu, B. Chen, D. Kalenichenko, W. Wang, T. Weyand, M. Andreetto, and H. Adam, "Mobilenets: Efficient convolutional neural networks for mobile vision applications," *arXiv preprint arXiv:1704.04861*, 2017.
- [21] T. Karras, S. Laine, and T. Aila, "A style-based generator architecture for generative adversarial networks," in *Proceedings of the IEEE/CVF conference on computer vision and pattern recognition*, 2019, pp. 4401–4410.
- [22] S. Hong, R. Marinescu, A. V. Dalca, A. K. Bonkhoff, M. Bretzner, N. S. Rost, and P. Golland, "3d-stylegan: A style-based generative adversarial network for generative modeling of three-dimensional medical images," in *DGM4MICCAI workshop in International Conference on Medical Image Computing and Computer-Assisted Intervention*. Springer, 2021, pp. 24–34.
- [23] A. Arnab, M. Dehghani, G. Heigold, C. Sun, M. Lučić, and C. Schmid, "Vivit: A video vision transformer," in *Proceedings of the IEEE/CVF International Conference on Computer Vision*, 2021, pp. 6836–6846.
- [24] A. Novikov, D. Podoprikin, A. Osokin, and D. P. Vetrov, "Tensorizing neural networks," *Advances in neural information processing systems*, vol. 28, 2015.
- [25] V. Lebedev, Y. Ganin, M. Rakhuba, I. Oseledets, and V. Lempitsky, "Speeding-up convolutional neural networks using fine-tuned cp-decomposition," *arXiv preprint arXiv:1412.6553*, 2014.
- [26] J. Kossaifi, A. Toisoul, A. Bulat, Y. Panagakis, T. M. Hospedales, and M. Pantic, "Factorized higher-order cnns with an application to spatio-temporal emotion estimation," in *Proceedings of the IEEE/CVF Conference on Computer Vision and Pattern Recognition*, 2020, pp. 6060–6069.
- [27] Y.-D. Kim, E. Park, S. Yoo, T. Choi, L. Yang, and D. Shin, "Compression of deep convolutional neural networks for fast and low power mobile applications," *arXiv preprint arXiv:1511.06530*, 2015.
- [28] K. Hara, H. Kataoka, and Y. Satoh, "Can spatiotemporal 3d cnns retrace the history of 2d cnns and imagenet?" in *Proceedings of the IEEE conference on Computer Vision and Pattern Recognition*, 2018, pp. 6546–6555.
- [29] F. N. Iandola, S. Han, M. W. Moskewicz, K. Ashraf, W. J. Dally, and K. Keutzer, "Squeezenet: Alexnet-level accuracy with 50x fewer parameters and 0.5 mb model size," *arXiv preprint arXiv:1602.07360*, 2016.
- [30] X. Zhang, X. Zhou, M. Lin, and J. Sun, "Shufflenet: An extremely efficient convolutional neural network for mobile devices," in *Proceedings of the IEEE conference on computer vision and pattern recognition*, 2018, pp. 6848–6856.
- [31] O. Kopuklu, N. Kose, A. Gunduz, and G. Rigoll, "Resource efficient 3d convolutional neural networks," in *Proceedings of the IEEE/CVF International Conference on Computer Vision Workshops*, 2019, pp. 0–0.
- [32] K. Weiss, T. M. Khoshgoftaar, and D. Wang, "A survey of transfer learning," *Journal of Big data*, vol. 3, no. 1, pp. 1–40, 2016.
- [33] Y. Wang, A. Gonzalez-Garcia, D. Berge, L. Herranz, F. S. Khan, and J. v. d. Weijer, "Minegan: effective knowledge transfer from gans to target domains with few images," in *Proceedings of the IEEE/CVF Conference on Computer Vision and Pattern Recognition*, 2020, pp. 9332–9341.
- [34] S. Chen, K. Ma, and Y. Zheng, "Med3d: Transfer learning for 3d medical image analysis," *arXiv preprint arXiv:1904.00625*, 2019.
- [35] K. He, X. Zhang, S. Ren, and J. Sun, "Deep residual learning for image recognition," in *Proceedings of the IEEE conference on computer vision and pattern recognition*, 2016, pp. 770–778.
- [36] M. Heusel, H. Ramsauer, T. Unterthiner, B. Nessler, and S. Hochreiter, "Gans trained by a two time-scale update rule converge to a local nash equilibrium," *Advances in neural information processing systems*, vol. 30, 2017.
- [37] C. Szegedy, V. Vanhoucke, S. Ioffe, J. Shlens, and Z. Wojna, "Rethinking the inception architecture for computer vision," in *Proceedings of the IEEE conference on computer vision and pattern recognition*, 2016, pp. 2818–2826.
- [38] I. Gulrajani, F. Ahmed, M. Arjovsky, V. Dumoulin, and A. C. Courville, "Improved training of wasserstein gans," *Advances in neural information processing systems*, vol. 30, 2017.
- [39] J. Wu, C. Zhang, T. Xue, B. Freeman, and J. Tenenbaum, "Learning a probabilistic latent space of object shapes via 3d generative-adversarial modeling," *Advances in neural information processing systems*, vol. 29, 2016.
- [40] M. Rosca, B. Lakshminarayanan, D. Warde-Farley, and S. Mohamed, "Variational approaches for auto-encoding generative adversarial networks," *arXiv preprint arXiv:1706.04987*, 2017.
- [41] G. Kwon, C. Han, and D.-s. Kim, "Generation of 3d brain mri using auto-encoding generative adversarial networks," in *International Conference on Medical Image Computing and Computer-Assisted Intervention*. Springer, 2019, pp. 118–126.